AMSR Precipitation Rate Retrieval Algorithm
--
Theoretical Basis and Operation

Grant W. Petty
Atmospheric and Oceanic Sciences
University of Wisconsin-Madison

1. Introduction

The Standard (pre-launch) Algorithm selected for over-ocean precipitation retrieval for the Advanced Microwave Scanning Radiometer (AMSR) is an adaptation of the algorithm developed for the Special Sensor Microwave/Imager (SSM/I) by Petty (1994a,b). The principle features that distinguish this algorithm from other rain rate algorithms include the following:

- Physical information concerning surface rain rate is supplied by the polarization difference at each frequency utilized in the inversion. As shown by Petty (1994a), a simple monotonic relationship exists between the local polarization difference and the total optical transmittance of the rain cloud at the frequency in question. The polarization difference is normalized with respect to a hypothetical cloud-free value under similar background conditions, thus eliminating variable water vapor and surface wind speed as important sources of systematic error in the retrieval.

- Scattering information at 89 GHz, as embodied by the *S* index of Petty (1994b), is postulated to contain only indirect information about surface rain intensity and it is therefore utilized only to generate the "first guess" rain rate field at high resolution. The first guess value at a local is modified only to the degree necessary to eliminate inconsistencies between calculated and observed polarization differences at the lower frequencies.

- The algorithm undertakes a spatial inversion of the polarization differences at the various frequencies utilized in the retrieval. That is, it iteratively seeks a high-resolution (5 km) rain rate field which is simultaneously consistent, to within specified tolerances, with the low-resolution fields of polarization difference observed at multiple frequencies. The disparate channel resolutions are explicitly accounted for in this inversion.

2. Algorithm Operation

2.1 Theoretical Basis

A number of factors make the optimal estimation of rain rate more difficult than the retrieval of many other parameters, such as column water vapor, column cloud water, etc. Examples include: (1) much larger optical thicknesses of precipitation and thus a high degree of non-linearity in both the forward and inverse problems; (2) the complexity of the interactions of microwave radiation (including scattering) with diverse liquid and frozen hydrometeors, whose physical and optical properties are highly variable in space and time; (3) the relative indirectness of the relationship between path-integrated cloud properties observable from space and surface precipitation rate; (4) the relatively poor spatial resolution of microwave radiometers compared with the horizontal scale of variability of rainfall; and (5) the highly 3-dimensional structure of many rain clouds. The last of these problems is further complicated by the oblique (55°) viewing angle of the AMSR, since it will often be emission from the sides and surface reflections of rain clouds, rather than their tops, that play a dominant role in FOV-averaged microwave radiances (Petty, 1994a; Petty *et al.*, 1994).

In view of the numerous physical and structural variables determining radiometer-observed brightness temperatures in any given pixel containing precipitation, it is important to make use of complementary information from as many channels as possible. It is further advisable to avoid attributing too great of precision to theoretically derived relationships, since such relationships generally do not allow for large departures of real rain clouds from common ideal assumptions, such as plane-parallel geometry.

The multichannel spatial inversion approach developed by Petty (1994b) attempts to achieve a balance between excessive reliance on uncertain physical models and excessive dependence on ad hoc statistical relationships and assumptions about beamfilling, etc. It attempts to maximize the use of the available information, but does so primarily by reference to observed path attenuation, rather than emission or scattering, so as to reduce the impact

of uncertainties in the properties of frozen hydrometeors aloft.

This method is unusual in explicitly solving for a high-resolution rain field which is simultaneously consistent with the observed low-resolution polarizations at all frequencies, after allowing for the overlap and varying size of the effective fields of view (EFOVs). It also makes generous allowance for uncertainties in the highly simplified forward model and for geophysical noise of other types; thus, forward calculations are not forced to exactly agree with the observations but rather are considered consistent if they fall within a specified range of the observed values for each relevant microwave frequency.

In order to adapt the Petty (1994b) rain rate algorithm to the AMSR, two major revisions were necessary: (1) modification of the assumed antenna pattern and overlap coefficients utilized in the spatial inversion, and (2) development of a simple forward model for predicting brightness temperatures and polarizations specifically at AMSR frequencies and viewing angles. Furthermore, because the original SSM/I version of the algorithm was designed to operate within a much larger specialized display and analysis program for that sensor, considerable rewriting and reorganization of the Glanguage code was necessary in order to repackage the algorithm as a self-contained subroutine (currently about 4000 lines of C and Fortran code).

2.1.1 *P* AND *S* INDICES

The foundation of the Petty (1994b) ocean rain rate algorithm lies in the use of polarization information to decouple scattering and attenuation information at a given microwave frequency. This information can then be utilized separately in the retrieval, weighted according to its relative directness as a measure of surface precipitation intensity.

As observed by the satellite, polarized brightness temperatures respond to uniform rainfall in the manner indicated by Fig. 1. For all frequencies, brightness temperatures first increase due to emission by rainfall as seen against a radiometrically cold ocean background. With increasing rain rate, saturation occurs first at the highest frequencies. At higher rain rates, scattering due primarily to large ice particles above the melting level begins to depresses brightness temperatures again. This effect is most pronounced at the highest frequencies, and its magnitude and spectral dependence is strongly dependent on assumptions about ice particle size and concentration above the melting level.

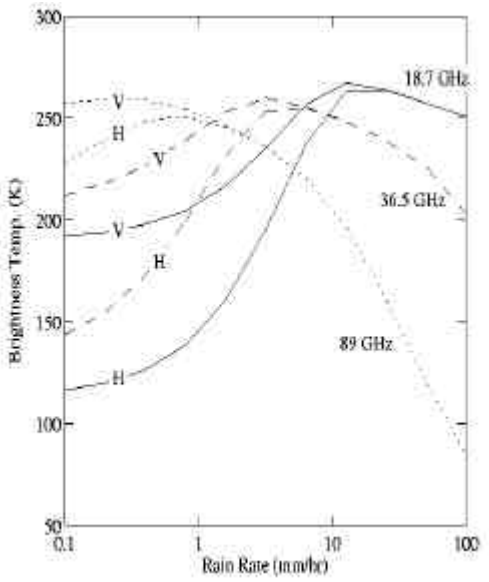

Figure 1: Idealized relationship between brightness temperature and surface rain rate for selected AMSR frequencies.

From this general behavior, it is clear that single-channel brightness temperatures from the AMSR yield an ambiguous measure of rain intensity, since it cannot be determined from the single brightness temperature whether one is on the left or right side of the peak for a given curve. Theoretically, one could resolve the ambiguity by using multiple frequencies at a single polarization, but this requires possibly unwarranted assumptions about the uniformity of rainfall within the widely differing FOVs of the respective channels.

When one considers the *difference* between the vertical and horizontal polarizations observed at a given frequency, the double-valuedness of the relationship disappears. The observed polarization difference $DT=T_V-T_H$

is essentially a monotonic measure of the visibility of polarized ocean surface emission through and between clouds and rain (this relationship breaks down somewhat in optically thick rain, owing to subtle effects by oriented ice particles). However, *DT* depends on other environmental properties as well, most notably total column water vapor *V* and surface wind speed *U.* It is therefore advantageous to define a so-called *normalized polarization P* as

$$P = \frac{\Delta T}{\Delta T_0(U,V,...)} \tag{1}$$

where DT_0 is the estimated cloud-free polarization difference at the time and location in question. The utility of this definition of *P* depends on one being able to make a reasonable estimate of *U* and *V* in locations of rainfall. This is accomplished either by direct retrieval from the AMSR data if the rain intensity is not too great or by interpolation into the rainy pixels from surrounding pixels.

Once *P* has been calculated for a given AMSR frequency, it serves as a physically direct index of total FOV-averaged path attenuation at that frequency due to clouds and rain only. It can be shown that, to a reasonable approximation (in view of many other unavoidable sources of error),

$$P \approx \tau^{\alpha} \tag{2}$$

in the case of horizontal uniform coverage by rain and cloud, where τ is the oblique-path microwave transmittance through the rain layer, and $\alpha \approx 1.7$ is approximately independent of frequency. Although a minor modification is required to account for the polarizing effects of ice particles in optically thick rain clouds, the above relationship serves as the primary basis for inferring rain intensity in a given FOV. Fig. 2 depicts *P* as derived from the dual-polarization brightness temperature curves appearing in the left panel of the same figure.

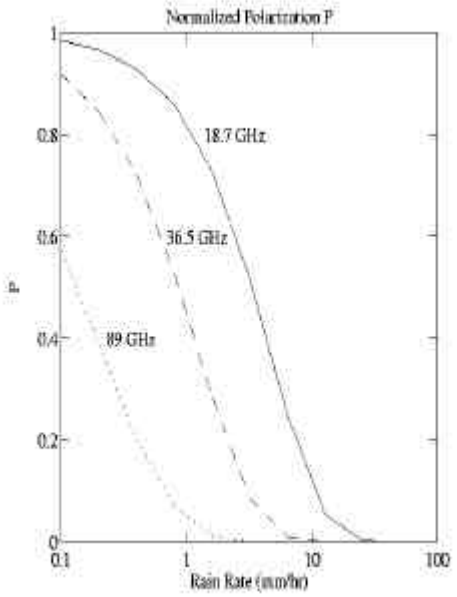

Figure 2: Idealized relationship between normalized polarization *P* and rain rate for selected AMSR frequencies.

Once a rain cloud becomes optically thick, the normalized polarization *P* saturates at a value near zero and yields no further information about surface intensity. Beyond that point, only the magnitude of the brightness temperature depression due to scattering by ice yields qualitative information about rain intensity. This information is indirect, because there is no unique relationship between the concentration and size of ice particles aloft and the intensity of surface precipitation. The so-called scattering signature is therefore weighted lightly in the algorithm, determining the surface rain rate only in cases where the estimate is not contradicted by evidence from the more physically direct *P*. In practice, this is accomplished by using the scattering information to specify the "first guess" rain rate and then modifying this rain rate estimate as necessary so as to eliminate inconsistencies with the observed *P* from the lower frequency channels.

As noted above, single channel brightness temperatures are ambiguous in that low values may imply either very light rain (and hence weak attenuation of the "cold" ocean surface emission or else heavy rain accompanied by much ice aloft. This ambiguity is again removed when one considers polarization in addition to brightness temperature: the unobscured ocean is "cold" but strongly polarized, whereas intense rainfall appears "cold" and only weakly polarized. The scattering index S for a given frequency is given by a linear combination of the vertical and horizontal polarized brightness temperatures. This index in effect compares the brightness temperature expected from a non-scattering, isothermal (T_C=273 K) cloud layer having the observed value of P with the observed brightness temperature. Thus,

$$S = P \cdot T_{V0} + (1 - P) \cdot T_C - T_V . \tag{3}$$

Fig. 3 depicts S as derived from the dual-polarization brightness temperature curves in Fig. 1.

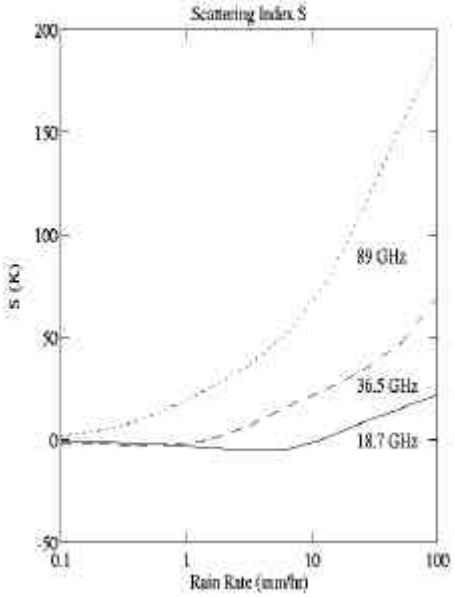

Figure 3: Idealized relationship between scattering index S and rain rate for selected AMSR frequencies.

Although all three frequencies show some scattering response to precipitation, only 89 GHz has a large enough response at modest rain rates to be routinely useful. Hence, S_{89} provides the first-guess rain rate R_0, based on the empirically determined linear relationship

$$S_{89} = C_S R_0 \tag{4}$$

A preliminary value of C_S is 2.9~K/(mm/h).

2.1.2 FORWARD MODEL

Although the relationship between P and total rain cloud transmittance τ is simple and relatively robust (for the horizontally homogeneous case), still needed is a model for the dependence of τ on rain rate R. We use the following expression

$$P_n = A_n \exp\left(-C_n Z_l R_n^B\right) \tag{4}$$

where Z_l is an effective rain layer depth (e.g. freezing level), and A_n, B_n, and C_n are frequency-dependent coefficients derived from theoretical calculations for a uniform Marshall-Palmer rain layer accompanied by an assumed 0.5 kg/m^2 of non-precipitating cloud water.

In the current version, Z_l is estimated empirically from the retrieved total column water vapor in the vicinity of

the raining pixel. The justification for this method, and the actual relationship, is given by Petty (1994b). In future versions, we may instead utilize either NWP model-analyzed freezing level or else lower tropospheric temperature estimates derived from the 50-53 GHz channels of the ADEOS-2 AMSR.

Because the above model relationship for P_n is based on highly simplified assumptions, it is treated as an approximation with fairly generous uncertainties. Only pixels whose forwarded-calculated P_n differs by more than a specified tolerance ΔP_n from the observed value are considered "inconsistent," thus requiring iterative modification of the retrieved rain rate field. However, when observed values of P from multiple channels are brought to bear, the requirement that the rain rate be consistent (to within tolerances) with all channels simultaneously constrains the retrieved rain rate rather effectively over a fairly wide range of intensities.

2.1.3 SPATIAL INVERSION

Not addressed so far is the problem of spatial inhomogeneity of rainfall within the respective fields-of-view (FOVs) of the channels used in the retrieval. Since each channel has a different resolution, one cannot assume that the same rain rate, or even that similar frequency distributions of rain rate, are present within each channel's FOV. Moreover, lower frequency channels have larger dynamic range (see Fig. 1) but lower sensitivity and also coarser spatial resolution than their higher-frequency counterparts. On the other hand, the coarser resolution FOVs overlap to a significant degree (i.e., are oversampled), suggesting the possibility of inverting the smoothed low-frequency polarization fields to obtain high-resolution rain fields. Such spatial deconvolution must be undertaken with care and with due consideration of the inherent ill-posedness of this kind of inverse problem in the presence of all forms of noise (instrument, geophysical, and that due to model errors).

The method developed by Petty (1994b) assumes that the rain rate is to be retrieved on a grid whose elements correspond to the positions of the high-resolution (89 GHz) channels' pixels. Unlike the 89 GHz FOVs, however, these grid elements, or retrieval cells, are contiguous and non-overlapping. Fig. 4 depicts the relationship between the fine-resolution rain rate retrieval grid and the effective FOVs of each relevant AMSR channel.

The observed P_{89} values are used to make an initial determination of whether rainfall is possible within a given high-resolution retrieval cell. If P_{89} is greater than a specified threshold, the pixel is deemed rain-free; otherwise it is flagged as "rain possible." The observed S_{89} value is then used to assign a first-guess rain rate to each cell identified as "rain possible," according to (4).

The next step is to forward-calculate the normalized polarization (P) field from the first-guess rain rate. This is accomplished by first computing local values P_i for each high resolution retrieval cell using (5), and then taking a weighted sum of these values within each FOV to derive an estimate of the low-resolution value of $\overline{P}$ corresponding to a given image pixel:

$$\overline{P_j} = \sum_i w_{i,j} P_j . \tag{6}$$

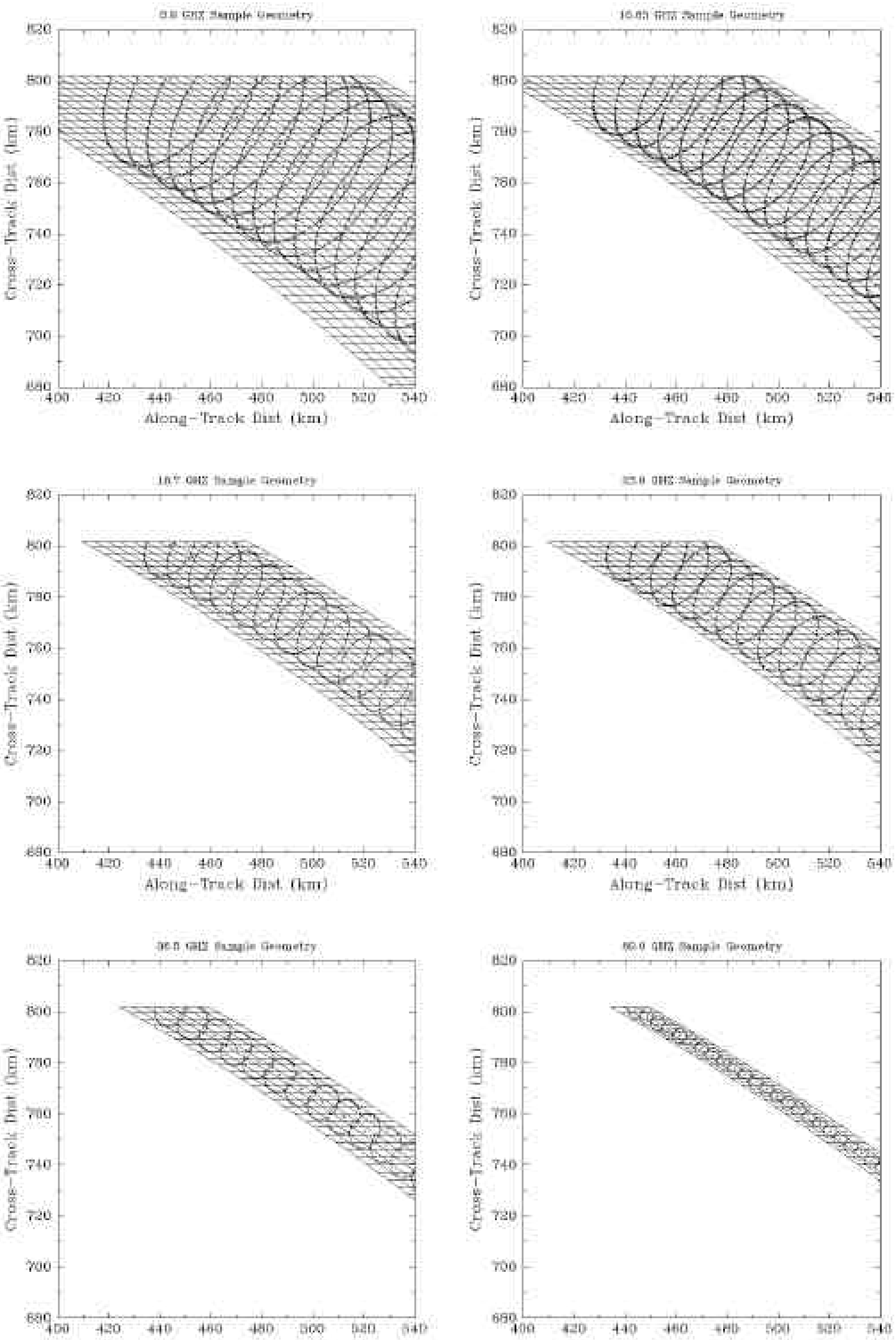
6.9 GHZ Sample Geometry
10.65 GHZ Sample Geometry
18.7 GHZ Sample Geometry
23.8 GHZ Sample Geometry
36.5 GHZ Sample Geometry
89.0 GHZ Sample Geometry
Cross-Track Dist (km)
Along-Track Dist (km)

Because the spatial relationship and degree of overlap between sensor pixels and retrieval cells is fixed at any point in a scan line, the coefficients $w_{i,j}$ are pre-computed for all channels and stored in arrays which are accessed by the algorithm during both the forward and inverse calculations.

For each sensor pixel for which the forward-computed $\overline{P}$ differs from the observed $\overline{P}$ by more than the specified tolerance *DP*, an adjustment is undertaken of the rain rates in the retrieval cells covered by that sensor FOV. Only retrieval cells identified as "rain possible" are candidates for adjustment. The magnitude of the adjustment is largest for the retrieval cells having the largest potential influence on the forward-calculated polarizations. Thus, where two different FOVs overlap a given retrieval cell, the one with the greatest sensitivity to changes in the rain rate in that cell will have the greatest control over the adjustment. Low sensitivity to changes in a given rain retrieval cell can be due either to saturation at the current-guess rain rate or else the position of the cell in the FOV.

The above adjustment is performed for all pixels flagged as "inconsistent" and this adjustment is performed in turn for each frequency utilized in the inversion (currently 18.7 and 36.5 GHz). The process is repeated a fixed number *N* times, after which it is assumed that no further improvement can be expected. Because of the differing resolutions and sensitivities of the different channels, it is rare that convergence, or near convergence, is not obtained at most locations, provided only that the tolerances are not set too tight. Optimal tolerances and iteration counts are best determined empirically, using real data where possible. For the SSM/I, $DP = 0.1$ and $N = 8$ yielded good results, but we are testing new values using the synthetic swath data supplied by NASDA/EORC.

3. Testing

Previous experience with this algorithm was based on the SSM/I version of the Petty (1994b) algorithm, which has been extensively intercompared with ground validation data in AIP-1, AIP-2, AIP-3, PIP-1, PIP-2, and PIP-3, as well as several "private" intercomparison studies. In the most recent two organized intercomparisons (AIP-3 and PIP-3), the results for the SSM/I version were very satisfactory by some measures. In particular, this algorithm had by far the highest instantaneous correlation with radar at 0.5° resolution in AIP-3. In PIP-3, it was one of the very few algorithms that simultaneously yielded good rms errors against monthly atoll rainfall amounts and also a high global time-space correlation with a ship-derived climatology of fractional-time-precipitating (Adler *et al.*, 2000).

Future testing plans include validation of the algorithm using data from the TRMM Microwave Imager (TMI), which is already flying and has many similar channels to AMSR. While the adaptation of the algorithm to TMI from AMSR will be much less arduous than was the adaptation from SSM/I to AMSR (since the previous adaptation was undertaken with future flexibility in mind), it is still a non-trivial task, owing to the need to derive yet another set of FOV overlap coefficients $w_{i,j}$ and other sensor-specific coefficients.

4. Known Issues and Future work

4.1 Scan geometry

A quantitative description of FOV overlap between adjacent pixels and between different channels of the AMSR was recently provided by EORC but has still not been incorporated into the algorithm. Antenna pattern overlap coefficients provided with current version are based on the assumption of Gaussian effective antenna weighting patterns.

4.2 Channel Usage

The present version utilizes only 18.7 and 36.5 GHz channels, corresponding to the original SSM/I channels of 19.35 and 37.0 GHz. Future versions may utilize 6.9 and 10.7 GHz channels as well, but the tradeoffs between computational effort, inversion stability, and retrieval performance improvement must be studied first.

4.3 Cloud free brightness temperatures

A prerequisite for the transformation of the raw polarized brightness temperatures into the *P* and *S* variables utilized in the physical inversion is a reasonably accurate estimate of the cloud-free brightness temperature in both vertical and horizontal polarization. Currently, this is achieved by first retrieving column water vapor *V* and

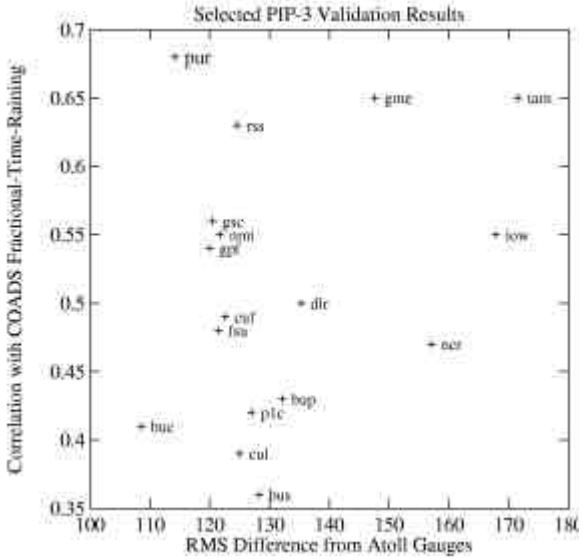

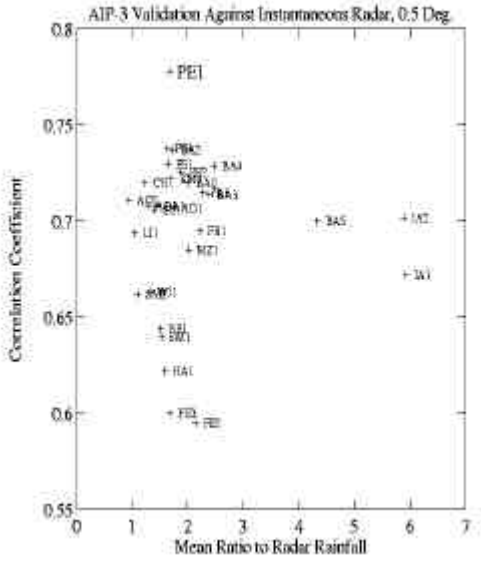

surface wind speed

Figure 5 (left): Validation results over 12 months (1992) of monthly rainfall products submitted to PIP-3. Only "pure SSM/I" algorithms are indicated in this figure. The horizontal axis indicates the RMS difference from atoll gauges. The vertical axis indicates the global correlation with ship-derived fractional-time-raining between 60S and 60N. Both sets of statistics were obtained from the PIP-3 Intercomparison Results volume. Only algorithms for which both statistics were available are included. The Petty (Purdue U.) physical algorithm is denoted "pur" in this intercomparison.

Figure 6 (right): Instantaneous validation results for SSM/I algorithms submitted to AIP-3, at 0.5 degree resolution. The horizontal axis depicts the mean ratio over the entire intercomparison period of the algorithm rainfall to the radar rainfall. The vertical axis depicts the correlation coefficient. Note that there is some uncertainty concerning the absolute calibration of the radar data – most algorithms (both SSM/I and IR) clustered around a ratio of approximately 1.5 to 2.5. The Petty physical algorithm was denoted "PE1" in this intercomparison.

U outside of areas of significant precipitation. These retrieved values are then interpolated into areas of precipitation and used to estimate cloud free brightness temperatures based on a simple empirical model which has again been adapted from the SSM/I.

For the pre-launch versions of the algorithm, it is necessary to extrapolate empirical relationship derived for the SSM/I to the slightly different frequencies and viewing angle of the AMSR. This extrapolation unavoidably depends on physical models whose absolute accuracy is imperfect. Consequently, we expect some systematic biases in the determination of cloud free radiances. This biases could in turn introduce errors or inconsistencies into the rain rate retrievals until the biases are corrected post-launch.

For the post-launch version of the algorithm, actual AMSR observations will be available in order to fine-tune both the *U* and *V* retrievals and the prediction of cloud-free T_B from *U* and *V*. Alternatively, the *U* and *V* values obtained from the Standard Algorithm for those variables may be utilized.

References

Adler, R., C. Kidd, G. Petty, M. Morrissey, and M. Goodman, 2001: Intercomparison of global precipitation products: The third precipitation intercomparison project (PIP-3). *Bull. Amer. Meteor. Soc.* (in press).

Petty, G., A. Mugnai, and E. Smith, 1994: Reverse Monte Carlo simulations of microwave radiative transfer in realistic 3-D rain clouds. In *7th Conference on Satellite Meteorology and Oceanography, Monterey, California, 6-10 June.*

Petty, G. W., 1994a: Physical retrievals of over-ocean rain rate from multichannel microwave imagery. Part I: Theoretical characteristics of normalized polarization and scattering indices. *Meteorology and Atmospheric Physics*, **54**(1-4), 79-100.

Petty, G. W., 1994b: Physical retrievals of over-ocean rain rate from multichannel microwave imagery. Part II: Algorithm implementation. *Meteorology and Atmospheric Physics*, **54**(1-4), 101-121.